AIAA-2001-4697

Crater and Rock Hazard Modeling for Mars Landing

Douglas E. Bernard and Matthew Golombek*

Landing on Mars is an extremely hazardous activity due to rough terrain that includes numerous craters at all scales. Mars also has widespread rock distribution, with many of those rocks created as a result of the cratering events.

Any mission attempting a landing on Mars must wrestle a number of questions such as what size rock and what slope the landing system must handle, whether the entire landed mission is compromised by landing inside a moderately small crater, and whether hazard avoidance during descent is required given the roughness of the target landing zone. If hazard avoidance is required, the engineers must determine how far must the descending vehicle translate to avoid typical hazards.

Answering these questions requires an understanding of the Mars topography including rocks and craters.

Earlier Mars orbiters and landers have provided sufficient information that crude models of the Mars surface may be constructed that allow an understanding of the engineering design trades involved in designing a Mars lander

These models include: models of crater number density vs. size for qualitatively different areas on Mars; models of how crater features scale with the size of the crater; models of rock coverage for different regions in and around a crater; and models of rock size distribution as a function of total rock coverage.

Based on these models, it is possible to examine trades involving the following engineering design parameters: size of landing ellipse; pre-selection of landing site to avoid large-scale hazards; translation required by a hazard avoidance system to avoid certain hazards; size of safe haven allowing hazard-free landing; and robustness of touchdown and surface operations system to hazards.

This paper describes these models and how they can be used to help understand these design trades.

INTRODUCTION

How hazardous is a planned Mars landing event? And if that is too hazardous, what actions can be taken to reduce the risk? For landing on Mars these questions are important to mission scientists and design engineers as well as Program and Project managers.

The question may be answered at many different levels of fidelity. In this paper, a low-fidelity approach is taken to allow the engineers and managers to understand the main design trades involved.

As a first step, let us reformulate the question for crispness and limit the scope:

Given a targeted landing site and known lander robustness to slope and rock landing hazards, estimate the likelihood of mission failure due to statistical crater and rock distributions.

An approach has been adopted that develops estimates of this likelihood based on inputs or assumptions covering the following:

- Mission Parameters
  - Statistical distribution of craters by size in landing site
  - Largest Crater in landing site
  - Smallest crater in which a successful mission can be accomplished
  - Ambient rock abundance in landing site
  - Largest rock that is not hazardous to the lander
  - Steepest slope that is not hazardous to the lander
- Crater Model
  - A model of how crater features scale with crater size

* Jet Propulsion Laboratory, California Institute of Technology.

- A model of how rock abundance varies in and around craters

- Rock Model
  - A model of how to estimate rock width distribution based on rock abundance
  - Typical rock height to width ratio

MARS CRATER DISTRIBUTION MODELS

Target Landing Sites

Consider the targeted landing ellipse:

Let A_{launch} be a region on Mars that represents the target landing site on launch day.

For MPF, MPL, and MER, this was an ellipse with a semi-major axis of 100-300 km. For second-generation landers, a capability of 3-6 km is intended to be available as early as 2007.

The surface of Mars is covered with a large number of craters compared to the surface of the Earth. Given the ubiquitousness of craters on Mars, there will be some distribution of craters in target landing sites as large as A_{launch}. The Project can choose to target more or less heavily cratered regions for landing.

For most landers, large craters are generally more hazardous to land on than small craters; and for landers with limited retargeting hazard avoidance capability, they are also more difficult to avoid. For these reasons, mission planners may find it advantageous to use pre-launch site surveillance to choose landing sites that are guaranteed to have no craters larger than a specified diameter.

Craters Size Frequency Distributions

Craters are ubiquitous on the surface of Mars. They have been observed at all scales from order thousand kilometers to a few meters diameter. Even if a landing ellipse is only a few kilometers in size, there will be craters within any ellipse, regardless of how the ellipse is selected. Crater number versus diameter relations for Mars based on the Viking Orbiter images of a few hundred meters per pixel show a fairly standard –2 slope distribution when plotted on a log-log plot of cumulative number of craters of a given diameter per million square kilometers versus diameter in kilometers [e.g., Strom et al., 1992[1]]. With the acquisition of high-resolution images of up to 1.5 meters per pixel by the Mars Global Surveyor, Mars Orbiter Camera, crater counts have been extended to diameters as small as ~10 m [Hartmann, 1999[2]]. Below 1 km diamter, Hartmann [1999] proposes a steeper distribution (by a factor of 2) of craters up to a saturation equilibrium that is similar to the –2 slope distribution. These distributions are shown in Figure 1 (denoted heavily, moderately and lightly cratered) and correspond to the 3 distributions shown in Hartmann et al. [1999[3]], which are suggested to be roughly a few billion, 100 million, and 10 million years old, respectively. Although there is some evidence that the craters extend in size below 10 m diameter [e.g., Horz et al., 1999[4]], the crater counts that have been done appear to show a rollover near this diameter [Hartmann et al., 1999, 2001[5]], suggesting that craters below this size may be destroyed by surface processes [Hartmann et al., 2001] or did not form (few can be identified from the landers). Even if the craters below 10 m diameter are not destroyed, crater depth/diameter relations discussed next indicate that they cease to represent a hazard as they are only a couple of meters deep. In addition crater counts for all but the youngest surfaces on Mars reported in Hartmann et al. [1999, 2001] and Hartmann [1999], tend to roll over at a maximum of about 10 craters per kilometer squared for diameters smaller than about 50 m, which may also be a result of covering of small craters by wind borne material. As a result for our models, we will not model craters with diameters smaller than 10 m and we will cap the incremental number of craters smaller than about 50 m diameter at 10/km^2. This is illustrated in Figure A. Craters up to only 1 km diameter are considered because for landing ellipses smaller than a few hundred km squared and the frequencies shown, it should be possible to select sites that do not have any craters larger than this diameter.

Based on that work, we define a set of Mars terrain* types chosen to span the range of cratering Hartman observed.:

• Lightly Cratered Terrain: characterized (for larger craters) by crater counts 1% of those seen on lunar plains. This model gives fewer craters at all sizes than all three of the regions considered in Hartmann et al. [1999].

• Moderately Cratered Terrain: characterized (for larger craters) by crater counts 10% of those seen on lunar plains.

• Heavily Cratered Terrain: characterized (for larger craters) by crater counts 100% of those seen on lunar plains. This model gives more craters for craters < 2 km

* Although the word "terrain" has terrestrial origins, we use it here to refer to a tract of land on Mars

in diameter than all three of the regions considered in Hartmann et al. [1999].

In Figure 1, we model crater distribution by grouping craters by size and counting the number of craters of a given size range or "bin." We adopt a bin size such that each succeeding bin is centered at a crater diameter that is the square root of two larger than the crater diameter for the previous bin center. Thus each bin collects craters ranging in size from 0.84 to 1.19 times the bin center value for diameter.

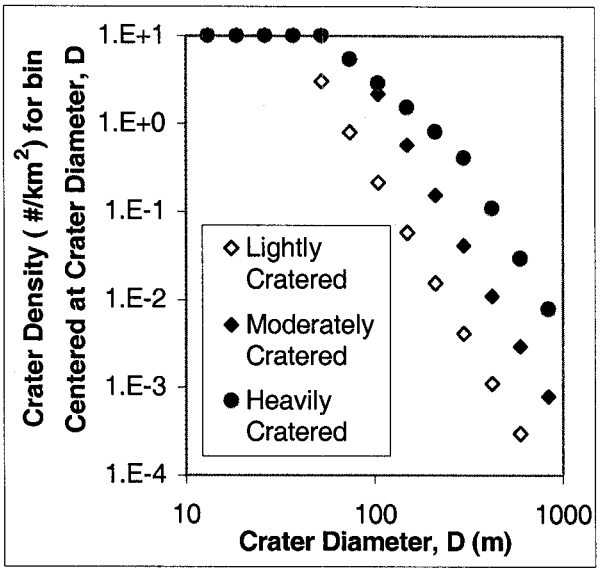

Figure 1. Crater Number Density Model

Largest Craters in a Landing Area

Consider different size landing ellipses. This defines an area. It may be desirable to avoid landing sites with large craters. Assume we allow exactly one crater larger than a given diameter in this area; what is that diameter? This may be determined from Figure 1.

We can usually expect to be able to position an error ellipse to avoid the largest craters in a region. (And with care, it may be possible to find an atypically crater free region in which to place the ellipse.) One number that is helpful in considering how difficult it is to place an ellipse in a region is the expected size of the second largest crater. Table 1 shows the size of this second largest crater for different size landing ellipse footprints. For scale, the MPF footprint was about 16,000 km^2. Second generation landers will be aiming for 10 to 100 km^2 size areas.

Table 1: Second Largest Craters in Landing Ellipse

	Diameter (m) of 2nd largest crater		
Area (km2)	Lightly Cratered	Moderately Cratered	Heavily Cratered
10	100	200	400
100	200	400	600
1000	420	600	1200
10000	600	1200	2400
100000	1200	2400	4800

From Table 1, we can conclude that it may be reasonable to insist on no craters larger than 500 m diameter in lightly cratered terrain for MPF-class landing footprints. For second generation landers, we may be able to choose a landing site with no craters larger than 200 m in diameter in lightly cratered terrain. In Moderately or Heavily Cratered terrain, we need to design for landing in regions with larger craters.

Area within Craters

The difference between lightly and heavily cratered regions becomes more apparent when the information if Fig. 1 is replotted in terms of the percent of the terrain that is enclosed by crater rims in each of the regions modeled above. This is shown in Fig. 2.

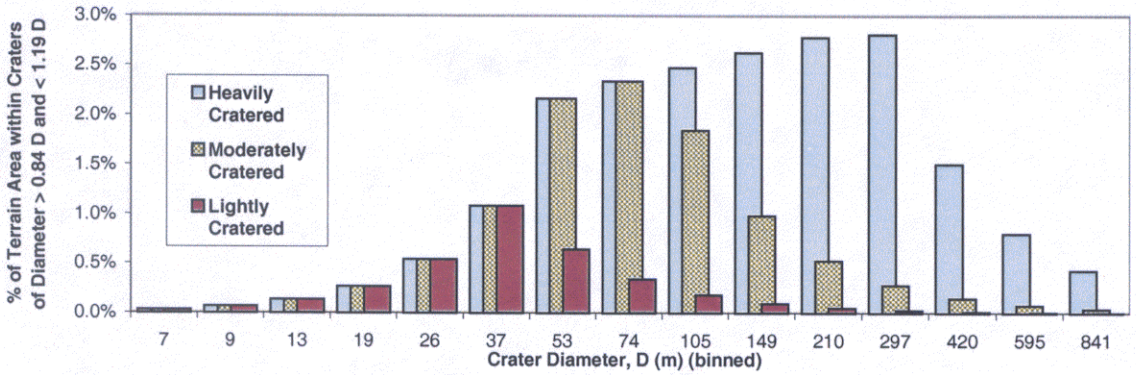

Figure 2. Areas Within Craters

MARS CRATER SCALING MODELS

Crater Shape

Craters below about 5-10 km in diameter have a well understood simple bowl shape with uplifted rim illustrated in Figure 3 with dimensions that scale with crater diameter [e.g., Melosh, 1989[6]]. Extensive measurements of lunar and Martian impact craters have shown that simple bowl shaped craters have depths that are 0.2 times their diameter, rims that are 0.04 times their diameter, a flat central floor, and an inner rim near the angle of repose (about 30°) [Pike, 1977[7]]. Measurement of the maximum blocks around fresh lunar craters suggests a relationship with the crater diameter. Although more complicated relationships have been suggested [e.g., Melosh, 1989], data in [Moore et al., 1969[8]] and the analysis by Gaskell [1993[9]] suggest the maximum block is roughly 0.02 times the diameter of the crater, which we will use herein.

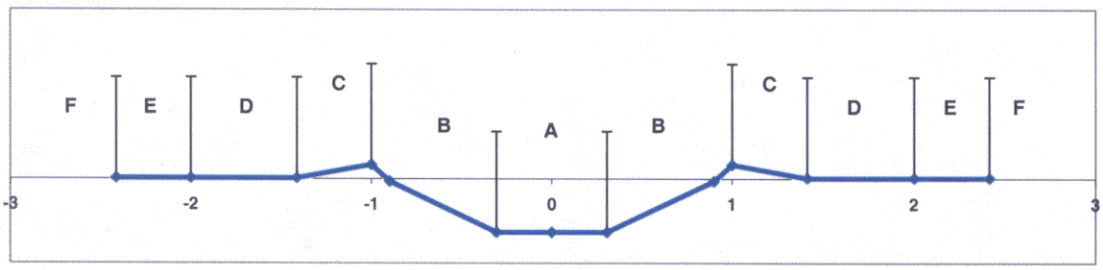

Figure 3. Crater Model Cross Section

Table 2 collects the scaling laws discussed above.

Rock Height

Rock heights have been measured at both Viking and the Pathfinder landing sites. Based on the Viking sites, Golombek and Rapp [1997[10]] found a weak dependence of rock height on total rock abundance, in which rock height is 0.36 versus 0.5 times rock diameter for total rock coverage of 6%, without the outcrops, versus 15% at Viking 1 versus Viking 2, respectively. Rock heights at the Mars Pathfinder site are about 0.5 times their diameter (where rocks cover 16% of the area [Golombek et al., 1997[11], 1999[12]]) and most rocky sites on the Earth reported on by Golombek and Rapp [1997] are the same. As a result in this analysis, we will assume rock height is 0.5 times diameter for simplification.

Table 2: Crater Scaling

Feature	Size, (% of D)
Diameter, D	100%
Maximum Depth	20%
Maximum Rim Height	4%
Maximum Rock Diameter	2%
Maximum Rock Height	1%

Rock Abundance Around Craters

A number of studies have been made of block distributions around craters on the lunar surface [e.g., Moore et al., 1969; Shoemaker and Morris, 1969[13]; Hutton, 1969[14]; Cintala and McBride, 1995[15]]. Craters produced by nuclear explosions on Earth clearly show that the distribution of rocks around craters depends on physical properties of the impacted material [Melosh, 1989]. Nevertheless there does appear to be a general decrease in both the total rock abundance as well as the maximum block size with distance from the crater. Fairly complex relationships have been suggested for this decrease [e.g., Gaskell, 1993] with distance. For this work we will use detailed counts of block abundance versus distance for fresh lunar craters to derive the total area covered by blocks as a general function of radius [Moore et al., 1969] and compare these distributions with an existing model for the size-frequency distribution of rocks on Mars [Golombek and Rapp, 1997], discussed in more detail later. The advantage of this approach is that it is based on the measured distributions, uses an existing model for rock distribution based on observations at the three landing sites on Mars and a variety of rocky locations on Earth that is based on fracture and fragmentation theory of rocks, and the distributions appear consistent with preliminary measurements in high-resolution Mars Orbiter Camera images of large blocks on the Martian surface in general and around Martian impact craters in particular [e.g., Golombek, 2001[16]]

The detailed block counts by Moore et al. [1969] on small (<1 km diameter), fresh lunar craters show that the total block abundance varies with the crater shape discussed above. Specifically, the blockiest areas are in the inner rim and on the rim where total rock coverage can be 40% or higher. The center of the crater has lower rock coverage (~20%), except in extremely blocky materials, and there is a general decrease in total block coverage with increasing radial distance from the rim (from ~30% at 1.5 times the radius to ~20% at 2 times the radius). An example of this behavior is illustrated in Figure A. In this illustration, areas within the 137 m diameter crater and within 1 radius of the crater rim have total rock coverage of about 40%. Beyond this rock coverage decreases with increasing distance from to 30% and 20%. The data from the 426 m diameter crater shows the low rock abundance on the central floor of the crater. Also shown in Figure 4, the distribution of rocks around fresh lunar craters compares favorably with models of rock distributions presented in Golombek and Rapp [1997] and the slopes of these curves.

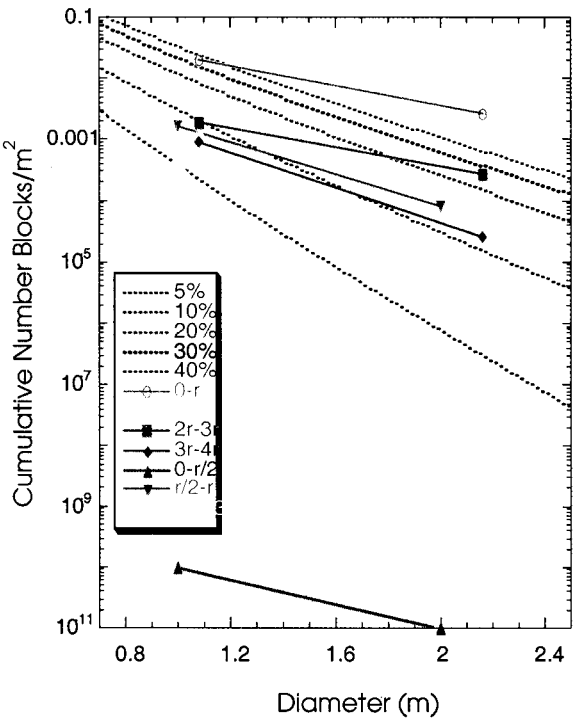

Figure 4. Plot of cumulative number of blocks of a given diameter or larger versus diameter for blocks around two lunar craters and rock size frequency distribution model. Dotted lines are the model rock size-frequency distributions for 5%, 10%, 20%, 30% and 40% total rock coverage numerically integrated to yield curves of cumulative number of blocks versus diameter as discussed in the text. Data shown are block distributions measured at various annuli around two fresh lunar craters. Data designated 0-r, r-2r, 2r-3r, and 3r-4r were measured around a 137 m diameter crater (IIIP9b) and data designated 0-r/2, r/2-r, and r-4r/3 were measured

around a 426 m diameter crater (IIIP8) as reported in Moore et al. [1969]. Data for the first crater show a drop in block abundance from roughly 0.001 blocks/m^2 with D>2.4 m for areas within 1 crater radius, consistent with the model distribution for 40% of the surface covered with rocks to about and order of magnitude less than this at distances greater than this, consistent with the model distribution for roughly 20% of the surface covered with rocks. Data for the second crater shows that the central floor of the crater (within a half crater radius) has few blocks, but block abundance peaks on the inner rim, and decreases away from the crater.

Crater Cross Section and Zone Definition

The rock and slope hazards vary considerably with location in or about a crater. To allow quantitative discussion of these locations and associated hazards, the following set of zones is proposed: Zone A is the nearly flat central region of a crater. Zone B is the inner slope of the crater rim and is further subdivided into B1, where the slope is approximately the 30° angle of repose and B2, at the rocky edge of the rim where slopes can exceed 30°. Zone C is the outer rim sloping down to the ambient terrain and has a heavy covering of rocks. Zone D is external to Zone C and has ambient slopes but still significant rock fields due to the crater. Farther out, Zone E has fewer rocks than Zone D. The rock coverage around the crater is modeled as starting at 40% at the crater rim and decreasing exponentially at a rate that drops the rock coverage by a factor of 2 for each additional crater radius of distance from the crater rim. Analysis of martian photos shows that the data could support a factor between 2 to 3. By chosing a factor of 2 here, we are erring on the side of modeling the crater as rockier than it may actually be. Table 3 captures the above Zone description in a quantitative manner.

Table 3: Crater Zones

Zone	Location	Rock Coverage	Slopes
A	Center to 0.3R	~20%	< 10°
B1	0.3R to 0.9R	~40%	<30°
B2	0.9R to 1.0R	40% to 100%	>30°
C	1.0R to 1.4R	40% to 30%	~10°
D	1.4R to 2.0R	30% to 20%	Ambient
E	2.0R to 2.4R	20% to 15% (or ambient)	Ambient
F	>2.4R	Ambient	Ambient

It will be seen later in this paper that the different zones represent quantifiably different risks to a lander.

The above scaling laws allow us to draw our "model crater" The reader is encouraged to note how simplified this model is and keep this in mind when interpreting the conclusions drawn using this model. See Figure 3.

Size of Zones

The crater distribution models of Figs. 1 and 2 may be combined with the zone definitions above to describe how much of the surface is in each zone different types of terrain. Figure 5 shows the size of each zone for lightly, moderately, and heavily cratered terrain.

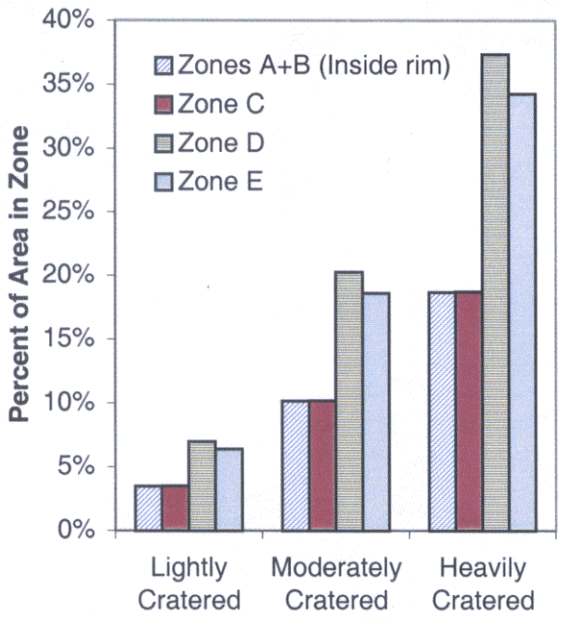

Figure 5. Areas of Zones A, B, C, D, E for Different Martian Terrains

MARS ROCK SIZE DISTRIBUTION MODELS

The information available on rock size distributions on Mars is very lean: we have estimates for Viking 1 and 2 and Mars Pathfinder sites only. Mars Global Surveyor caries a thermal mapper that is able to characterize areas on Mars in terms of gross rock coverage: the fraction of the measured surface covered by rocks greater than a certain (sub-centimeter) size. The measurement depends on the thermal inertia of rocks vs. sand. Hazardous rocks comprise 7% of the surface area at the Viking 1 site and 18% at the Viking 2 site. These percentages are sometimes referred to as rock coverage or rock abundance. In the modeling to follow, this information will be extrapolated to rock coverages of higher rock abundance. Note that the further from the 7-18% data we extrapolate, the less secure the model results.

Rock Size-Frequency Data and Model

The size-frequency distribution of rocks have been analyzed from lander images at the two Viking landing sites and at the Mars Pathfinder landing site. Rock distributions within the near fields (<10 m from the landers) of the Viking 1 and 2 landing sites were produced by Moore et al. [1979[17]] and Moore and Keller [1990[18], 1991[19]]. Based on these measurements, measurement of rocks in the far field of Viking Lander 1, and a number of rocky locations on Earth, Golombek and Rapp [1997] derived a model that describes the rock size-frequency for any total rock abundance estimated from thermal measurements of Mars [e.g., Christensen, 1986[20]]. The model proved correct at predicting the observed size-frequency distribution of rocks at the Mars Pathfinder landing site [Golombek et al., 1999]. The rock distribution has been counted in a 3-6 m annulus around the Pathfinder lander for the 30-day report [Golombek et al., 1997] (representing a preliminary product) and the far field (>10 m from the lander) [Haldemann et al., 2000[21]], but we have not yet completed the near field. Consequently, we will base our derivations on the Viking data [Moore and Keller, 1990, 1991], but will show the preliminary data from near field and the far field at the Pathfinder [Golombek et al., 1997] and Viking 1 landing sites for comparison [Golombek and Rapp, 1997].

The model of the cumulative area covered by rocks of a given diameter or larger F(D) is an exponential of the form:

$$F_k(D) = k \exp [-q(k) D] \quad (1)$$

where D is rock diameter, k is the total area covered by rocks of all sizes (the total rock coverage), and q(k) is the exponential factor. Fits to the Viking lander 1 and 2 data yield k_1=0.069, q_1=4.08; and k_2=0.176, q_2=2.73. There are two equations and two unknowns, allowing derivation of a function relating q(k) and k of

$$q(k) = 1.863 + 0.153/k \quad (2)$$

Model rock abundances for different values of the total rock abundance were calculated from the solutions to k and q in equation 1 [Golombek and Rapp, 1997] and are illustrated in Figure 6. As can be seen in Figure 6, even though the model is based on rock distributions at the Viking landing sites, it does an excellent job describing the Mars Pathfinder rock distributions as well and can be used until the near field rocks are completely counted.

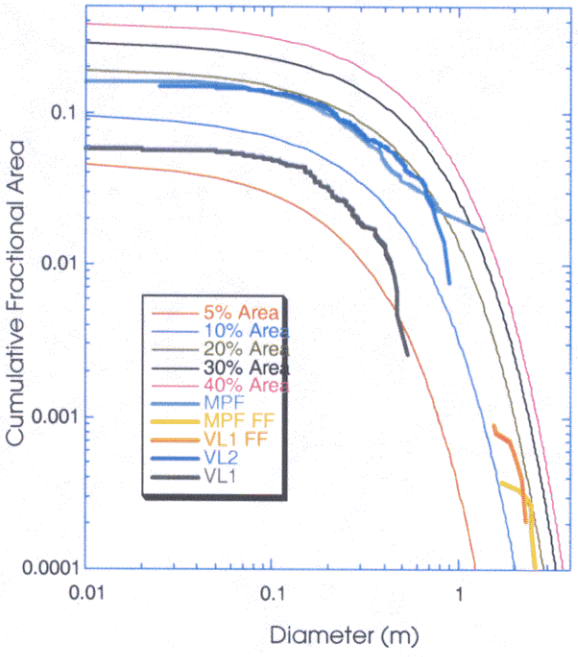

Figure 6: Plot of cumulative fractional area covered by rocks of a given diameter versus diameter for model size-frequency distributions proposed for Mars by Golombek and Rapp [1997] for 5%, 10%, 20%, 30% and 40% total area covered by rocks (equation 1) and data for the Viking 1 and 2 lander near fields (VL1 and VL2) [Moore and Keller, 1990, 1991], the 3-6 m annulus around Mars Pathfinder (MPF) [Golombek et al., 1997], and the far fields of Viking lander 1 (VL1 FF) [Golombek and Rapp, 1997] and Pathfinder (MPF FF) [Haldemann et al., 2000] for rocks greater than 1.5 m diameter. Even though near field data of Mars Pathfinder is skewed due to the inclusion of one large rock (Yogi) in a small counting area, the far field data using the triangulation method [Haldemann et al., 2000] is consistent with that expected for a region with just below 20% total area covered by rocks. Far field data from Viking lander 1 include ejecta and rim blocks from a crater, so the total area covered by rocks is greater than the near field, but the overall distribution is consistent with the model predictions.

One of the difficulties of using the model rock abundances is that they were cast in terms of the cumulative area covered by rocks greater than a given diameter versus diameter (equation 1) and many engineering applications require the cumulative number of rocks greater than a given diameter versus diameter. The simplest method for generating rock abundances in terms of the cumulative number that is identical to cumulative area distribution is to numerically integrate the cumulative area curves. This is illustrated in Figure 7, which shows the cumulative number of rocks greater than a given diameter versus diameter. These curves were derived by numerically calculating the cumulative area covered by rocks (from equation 1) in small increments, determining the area covered in small diameter bins, and determining the number of rocks of that bin diameter needed to produce the area covered by these rocks.

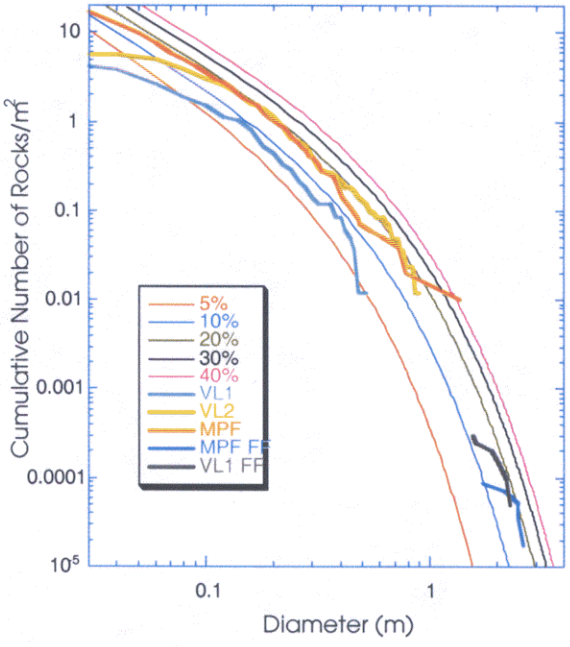

Figure 7: Cumulative number of rocks per square meter of a given diameter or larger versus diameter plot of model rock distributions and data from the three landing sites on Mars. Model rock distributions for 5%, 10%, 20%, 30% and 40% total area covered by rocks were derived by numerically integrating the cumulative area function (equation 1) in small diameter increments. Data for the three landing sites are the same as described in Figure 1. Models describe the rock distributions well for diameters greater than 0.1 m. The far field distribution of data for the Mars Pathfinder site fall very near that predicted by the model.

As can be seen from Figure 2, the simple numerical integration of the cumulative area function fits the observed rock distributions at the three landing sites

quite well for diameters greater than 0.1 m at the 2 Viking landing sites and a diameters greater than 0.05 m at the Pathfinder landing site (the Pathinder site does contain more pebbles than either Viking site). This discrepancy is real. The total number of rocks should reach a maximum at diameters near 1 cm (see discussion in Golombek and Rapp [1997] and Malin [1988[22], 1989[23]], but the model curves derived in this manner do not. The reason the curves do not is that they are not actually exponentials. Golombek and Rapp [1997] show that going from the cumulative number versus diameter distributions to the cumulative area versus diameter distributions in a mathematically rigorous way actually introduces a quadratic equation into the relationship (see equations 5-10 in Golombek and Rapp [1997]). Because of this, simply taking the cumulative number relations and determining the number of rocks in small diameter bins and multiplying the number of rocks of a given size by the area of a rock of this size will underestimate the area covered by rocks of that size. There is no analytic way to go from the cumulative area relationship to a cumulative number relationship (a difficulty of using exponential functions over simple power law relationships proposed previously (see discussion in Golombek and Rapp [1997]). For our analysis, we will use these numerically integrated curves for rock diameters greater than 0.1 m diameter for deriving the number of rocks of a given size or larger for areas of different total fractional rock coverage.

Applying a block height of half the block diameter and plotting the above against rock height gives Figure 8 as a function of rock coverage.

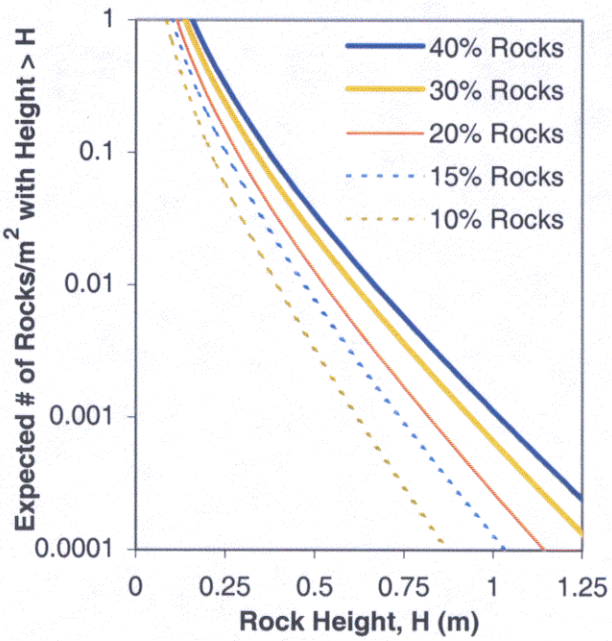

Figure 8. Rock Distribution by Height

ROCKS AND ZONES

It is instructive to compare expected number of large rocks in the different zones of a crater as defined in Table 3. Figure 9 plots the ratios of the numbers of tall rocks per square meter of each zone compared to zone C. The definition of he height of a tall rock is chosen as the independent variable. Note that Zone E corresponds roughly with the rock distribution seen in both the Viking 2 and the Mars Pathfinder landing sites.

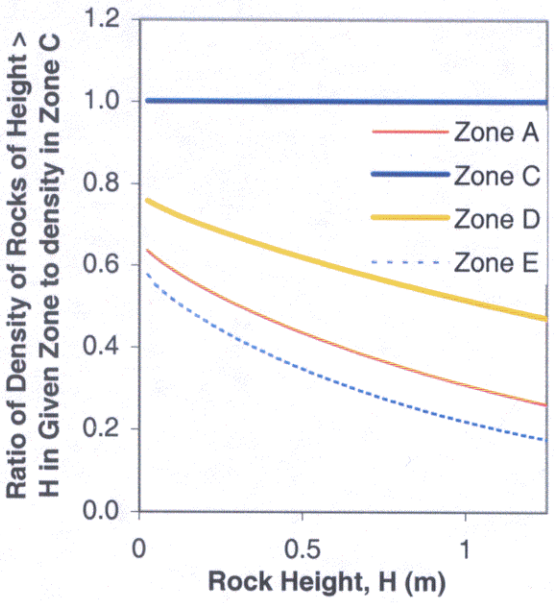

Figure 9. Tall Rock Ratios for Crater Zones

Given the rock number densities derived above, the Expected number of rocks in the projected area of any lander approaching the surface of Mars may be determined.

The upcoming MER mission is expected to have a diameter of approximately 1.3 m (5-6 m with the airbags inflated). The Mars '07 Smart Lander is expecting a diameter of about 5 m and future Mars Sample Return missions are likely to be the size of the smart lander or a bit larger. Figure 10 shows the expected number of tall rocks within the lander projected area for several values of lander diameter spanning the space of near future landers.

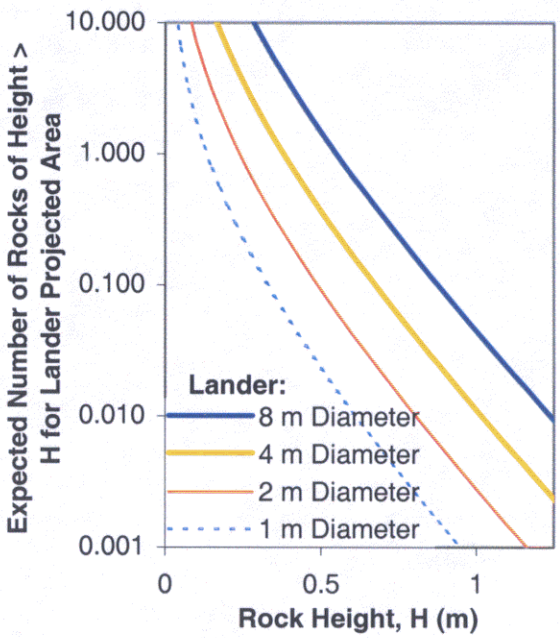

Figure 10. Tall Rocks in Zone C

From Figure 10 we see that a 5 m diameter lander landing in Zone C has about a 2% chance of landing on a rock that is 1 m or greater in height. Note how much improved this situation is from that when we need to be concerned about rocks that are greater than 0.5 m in height. The expected number of rocks of this height for a 5 m diameter lander is 0.6.

Figures 7 and 8 may be used together to determine the probability of rocks when landing in Zones A, D and E respectively.

\$ GG□ D□ ILJXUH□ GNH□ ³ 5 HGJUHQ HQZ □ FUDVK DJDLQVW □

Example Hazard calculation

The above discussion is sufficient to take a rough cat at hazard assessment for a given landing terrain and a given lander size and robustness. As an example, assume we are landing in lightly cratered terrain with with no craters larger than 600 m in diameter using a lander of 1.25 m diameter which is capable of handling < 1 m rocks and < 30 degree slopes. Assume also that the ambient rock abundance is 15%. And ambient slopes are < 10 °

The 1 m rock capability matters in several ways: first, craters < 5 m in diameter have crater rims smaller than the allowable rock size, so they pose no hazard at all. Since craters < 100 m do not create additional rocks larger than 1 m, these craters have slope hazards, but no rock hazards.

Table 4: Rock and Crater Hazards

Craters	D < 5 m	5 < D < 100 m			100 m < D < 600 m						None
Zone	A-E	B1	B2	A, C-E	A	B1	B2	C	D	E	F
% Area Covered	0.02	2.2	0.6	20	.04	.3	.07	.4	.8	.7	.78
Rocks					20%	40%	100%	35%	25%	17.5%	15%
Expected # of hazardous rocks under lander	.003	.021	>1	.003	.005	.021	>1	.017	.009	.004	.003
Probability of 1 or more hazardous rocks under lander	.003	.021	1	.003	.005	.021	1	.017	.009	.004	.003
Slopes		30°	> 30°	< 10 °	< 10 °	30°	> 30°	< 10 °	< 10 °	< 10 °	< 10 °
Slope a hazard for this lander?	N	Y	Y	N	N	Y	Y	N	N	N	N
Probability of hazardous rocks or slope	.003	1	1	.003	.005	1	1	.02	.01	.004	.003
Product of area fraction times hazard probability		.022	.006	.005	-	.003	.0007	.00008	.00008	.0000 3	.0023

Inspecting Table 4 shows that for this combination of landers and terrains, the Area B slope hazard is the most significant hazard, followed by the ambient (Zone F) rock hazard. Supping across all the different zones for different size crater regions gives **a total 4% chance of landing on unacceptable slopes or rocks [rewrite with another illustrative example?].** A design that could accommodate the 30% slope of zone B1 could eliminate more than half of this risk.

HAZARD AVOIDANCE

Since significant crater and rock hazards are found in most places of interest on Mars, and since landing on them with no ability to avoid the rock and slope hazards creates a substantial risk of mission failure. Designers of future mars landing missions are considering options for active terminal hazard avoidance. Active hazard avoidance refers to the activity of observing the site the lander is approaching, and autonomously modifying the flight path of the lander to avoid observed hazards. Terminal hazard avoidance refers to hazard avoidance during the terminal descent phase of entry descent, and landing.

With Active terminal hazard avoidance, the odds of surviving a ladning in hazardous terrain may be improved. Assume that the hazard avoidance system performs flawlessly and that rock hazards from one touch-down site to another in a given zone are uncorrelated. In this situation, there is a simple relation between the expected number of hazardous rocks within the an area equal to the cross-sectional area of the lander and the probability of mission failure due to these hazardous rocks.

Let N_{HR} be the expected value of the number of hazardous rocks in an area the size of the projected horizontal area of the lander.

Let m be the number of independent sites reachable by a hazard avoidance system.

Let P_{MF} be the probability of mission failure due to landing on hazardous rocks (evaluated for a given zone).

Then:

$$P_{MF} = (1\text{-}exp(N_{HR}))^m \qquad (3)$$

Note that for {m = 1} and {$N_{HR} << 1$ }, equation 3 above may be approximated by: $P_{MF} = N_{HR}$.

Equation 3 is plotted for a variety of values of m in Figure 11.

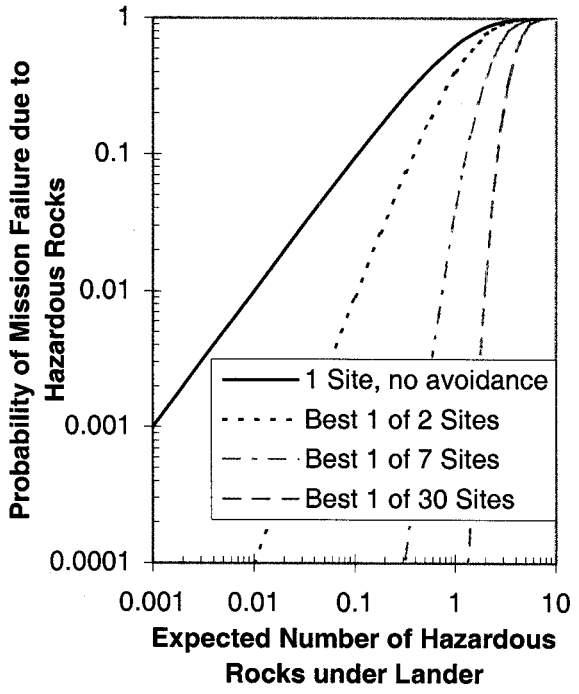

Figure 11. Hazard Avoidance and Mission Success for landing in any given Hazard Zone

HORIZONTAL TRANSLATION

Within a given hazard zone, for low probabilities of hazardous rocks, the probability of mission failure can be significantly reduced by hazard avoidance systems that are as simple as choosing the best of 2 sites. As the expected number of hazardous rocks increases, reasonable failure probabilities may require several or many options from a hazard avoidance system. As the expected number of rocks per site exceeds 2-3, it becomes difficult to find a safe spot to land even with many spots to choose from. So for rock avoidance where the specific hazards are uncorrelated, a hazard avoidance system that translates one to three lander diameters should be sufficient.

The reason to consider greater horizontal translation capability is the desire to avoid some zones entirely. For example, we may want the ability to translate far enough to avoid crater rims hazards.

How far is far enough? That depends on several considerations:

- Which Zones of a crater are to be avoided?
- How large a crater must be considered?
- Is it sufficient to avoid the crater rim or must the entire crater be avoided?

Figure 12 plots the linear relationship between crater diameter and the horizontal translation that is required to escape from the indicated zones. Consider the example where we are concerned about craters of diameter less than 300 m only. If we design our hazard avoidance system to avoid Zone B, we require a horizontal translation capability of about 50 m. Note that if we choose to avoid landing inside small craters (Zones A and B), this 50 m translation capability is enough to allow us to avoid landing in craters of 100 m diameter or less. Note that Figure is independent of how heavily cratered the terrain is with one caveat: the figure assumes that there is only one hazardous crater requiring terminal avoidance. This assumption needs to be revisited for landing in heavily cratered terrain or when landing systems with low landing robustness for which even small craters are hazardous.

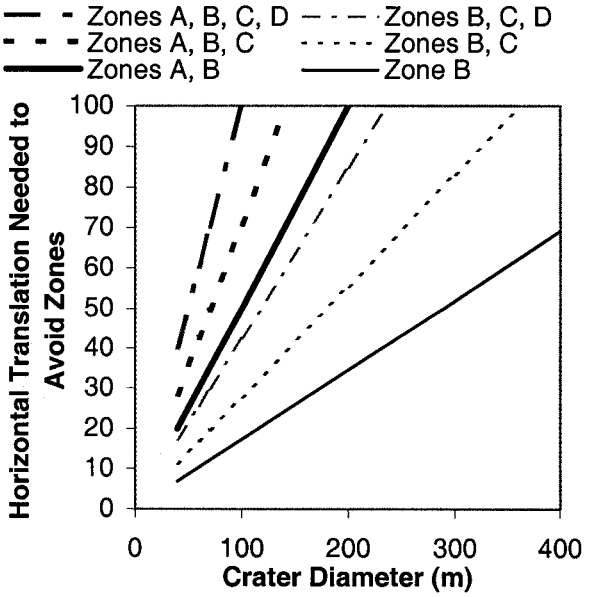

Figure 12. Horizontal Translation to Escape Crater Zones

SUMMARY

The work presented here may be used as a rough starting point to compare conceptual design approaches. Once an approach has been selected, much higher fidelity modeling is required to determine actual level of risks posed by rocks and craters.

ACKNOWLEDGEMENTS

This paper describes work performed at the Jet Propulsion Laboratory, California Institute of Technology, under contract from the National Aeronautics and Space Administration.

REFERENCES

[1] Strom, R. G., S. Croft, and N. Barlow, 1992, The Martian impact cratering record, in MARS, Kieffer, H. H., Jakosky, B. M., Snyder, C. W., and Matthews, M. S., eds., University of Arizona Press, Tucson, pp. 383-423.

[2] Hartmann, W. K., 1999, Martian cratering VI: Crater count isochrons and evidence for recent volcanism from Mars Global Surveyor, Meteoritics and Planetary Science, v. 34, p. 167-177.

[3] Hartmann, W. K., M. Malin, A. McEwen, M. Carr, L. Soderblom, P. Thomas, E. Danielson, P. James, and J. Veverka, Evidence for recent volcanism on Mars from crater counts, Nature, 397, 586-589, 1999.

[4] Horz, F., M. J. Cintalla, W. C. Rochelle, and B. Kirk, 1999, Collisionally processed rocks on Mars, Science, v. 285, p. 2105-2107.

[5] Hartmann, W. K., J. Anguita, M. A. de la Casa, D. C. Berman, and E. V. Ryan, 2001, Martian cratering 7: The role of impact gardening, Icarus,, v. 149, p. 37-53.

[6] Melosh, H. J., 1989, Impact Cratering, A Geologic Process, Oxford Univ. Press, New York, 245 pp.

[7] Pike, R. J., 1977, Size-dependence in shape of fresh impact craters on the Moon, in Impact and Explosion Cratering, eds. D. J. Roddy, R. O. Pepin, and R. B. Merrill, pp. 489-509, Pergamon Press, NY.

[8] Moore, H. J., R. J. Pike, and G. E. Ulrich, Lunar terrain and traverse data for lunar roving vehicle design study, Prelim. U. S. Geol. Surv. Rep., March 19, 1969.

[9] Gaskell, R., 1993, Martian Surface Simulations, Journal of Geophysical Research, v. 98, p. 11,099-11,103.

[10] Golombek, M., and Rapp, D., 1997, Size-frequency distributions of rocks on Mars and Earth analog sites: Implications for future landed missions: Journal of Geophysical Research, v. 102, p. 4117-4129.

[11] Golombek, M. P., Cook, R. A., Economou, T., Folkner, W. M., Haldemann, A. F. C., Kallemeyn, P. H., Knudsen, J. M., Manning, R. M., Moore, H. J., Parker, T. J., Rieder, R., Schofield, J. T., Smith, P. H., and Vaughan, R. M., 1997, Overview of the Mars Pathfinder mission and assessment of landing site predictions: Science, v. 278, p. 1743-1748.

[12] Golombek, M. P., Moore, H. J., Haldemann, A. F. C., Parker, T. J., and Schofield, J. T., 1999, Assessment of Mars Pathfinder landing site predictions: Journal of Geophysical Research, v. 104, p. 8585-8594.

[13] Shoemaker, E. M., and E. C. Morris, Size-frequency distribution of fragmental debris, in Surveyor Program Results, NASA Spec. Pub. 184, pp. 82-96, 1969.

[14] Hutton, R. E., Lunar surface models, NASA SP-8023, 55pp., 1969.

[15] Cintala, M. J., and K. M. McBride, Block distributions on the lunar surface: A comparison between measurements obtained from surface and orbital photography, NASA Tech. Mem. 104804, 41pp., October 1995.

[16] Golombek, M. P., 2001, Extreme rock distributions on Mars (expanded abstract): Lunar and Planetary Science XXXII, Abstract #1116, Lunar and Planetary Institute, Houston (CD-ROM).

[17] Moore, H. J., C. R. Spitzer, K. Z. Bradford, P. M. Cates, R. E. Hutton, and R. W. Shorthill, Sample Fields of the Viking Landers, J. Geophys. Res., 84, 8365-8377, 1979.

[18] Moore, H. J. and J. M. Keller, 1990, Surface-material maps of the Viking landing sites on Mars (abs.), NASA Tech. Mem. 4210, Rep. Planet. Geol. Geophys. Prog. - 1990, 160-162.

[19] Moore, H. J. and J. M. Keller, 1991, Surface-material maps of the Viking landing sites on Mars (abs.), NASA Tech. Mem. 4300, Rep. Planet. Geol. Geophys. Prog. - 1989, 533-535.

[20] Christensen, P. R., The spatial distribution of rocks on Mars, Icarus, 68, 217-238, 1986.

[21] Haldemann, A. F. C., Forsberg, N. K., Golombek, M. P., and Bridges, N. T., 2000, Far-field rock size-frequency distribution at the Mars Pathfinder landing site and comparison to the near field (expanded abstract): Lunar and Planetary Science XXXI, Abstract #1846, Lunar and Planetary Institute, Houston (CD-ROM).

[22] Malin, M. C., Rock populations as indicators of geologic processes (abs.), NASA Tech. Mem. 4041, Rep. Planet. Geol. Geophys. Prog. - 1987, 502-504, 1988.

[23] Malin, M. C., Rock populations as indicators of geologic processes (abs.), NASA Tech. Mem. 4130, Rep. Planet. Geol. Geophys. Prog. - 1988, 363-365, 1989.